Clays Clay Miner., Vol. 71, No. 4:461–477, 2023
https://doi.org/10.1007/s42860-023-00252-6

ORIGINAL PAPER

Preparation and Corrosive Anion-curing Capability of Layered Double Hydroxide (LDH)/Montmorillonite Composites

Limei Wu · Mingxi Sun · Xiaolong Wang · Yushen Lu · Ning Tang · Lili Gao · Qing Wang · Ling Hu

Accepted: 17 August 2023 / Published online: 14 September 2023

Abstract The passive film of reinforcing steel in marine concrete is damaged by the infiltration of chloride and sulfate ions. Layered double hydroxide (LDH) can adsorb anions and release interlayer ions to form passive films due to its ion exchange property. A Mg-Al-NO_3 layered double hydroxide/montmorillonite (LDH/Mnt) composite inhibitor was prepared by layer-by-layer self-assembly (LBL) of LDH and Mnt. The structure and morphology of the LDH/Mnt composites were characterized by X-ray diffraction (XRD), laser Raman spectroscopy, N_2-adsorption/desorption measurements, and transmission electron microscopy (TEM). The LDH/Mnt composites, as inhibitors of chloride ions and sulfate ions, exhibited high slow-release efficiency. The mass ratio of LDH and Mnt affected the curing capacity of the synthesized composites, and the optimum mass ratio was LDH/Mnt = 1:1 for which slow-release efficiency reached 94.16%.

Keywords Corrosion protection · Inhibitor · Layer double hydroxides · LDH/Mnt composite · Nitrate ions

Introduction

In recent years, as the development of global land resources has become saturated, many countries have focused on vast ocean resources (Geoffrey & Nicholas, 2008; Kim, 2009; Odeku, 2021). The exploitation of ocean resources is based on the construction of ocean engineering, and the role of marine concrete is important in the process of ocean engineering construction. The passive film on the surface of reinforcing steel in concrete will be damaged in seawater and sea sand environments due to the continuous infiltration of chloride ions and sulfate ions, leading to severe corrosion (Wang et al., 2017; Machner et al.,

Associate Editor: Binoy Sarkar.

L. Wu (✉) · M. Sun · N. Tang (✉) · L. Gao · Q. Wang
School of Materials Science and Engineering, Shenyang Jianzhu University, Shenyang 110168, China
e-mail: lmwu@sjzu.edu.cn

N. Tang
e-mail: tangning@sjzu.edu.cn

X. Wang
School of Mechanical Engineering, Shenyang Jianzhu University, Shenyang 110168, China

Y. Lu
Key Laboratory of Clay Mineral Applied Research of Gansu Province, Center of Eco-material and Green Chemistry, Lanzhou Institute of Chemical Physics, Chinese Academy of Sciences, Lanzhou 730000, People's Republic of China

L. Hu
Planning and Finance Division, Shenyang Jianzhu University, Shenyang 110168, China

2018). At the same time, the diffusion of carbon dioxide will reduce the pH of concrete pore solution (Tian et al., 2019), resulting in further aggravation of rust.

A survey found that exposure to the oceanic atmosphere caused >40% of the buildings to be affected in a coastal town near Valencia, Spain (Adam et al., 2016). In the United States, where a large number of bridges are made of concrete, 70,000 are structurally deficient, and >15% are at risk of corrosion (Valdez et al., 2016). The research on corrosion resistance of marine concrete is important for the exploitation of ocean resources.

Adsorption of corrosive anions is a solution for adapting concrete to seawater and sand environments. As an inhibitor, layered double hydroxide (LDH) has garnered significant research attention due to its excellent ion exchange properties (Wang & O'Hare, 2012; Zubair et al., 2017). LDHs are anionic clays and their interlayer ions are connected to the lamellae by weak hydrogen bonds (Rives & Angeles Ulibarri, 1999; Qiu et al., 2006; Ahmed & Gasser, 2012), which other environmental anions can replace easily, e.g. chloride ions and sulfate ions (Acharya et al., 2007; Daud et al., 2019; You et al., 2001). The key parameters of LDH as an anionic inhibitor are the surface charge, specific surface area, and pore-size distribution, which determine the type of anions preferred for the adsorption/intercalation process. LDH materials of lower surface charge density, but larger pore sizes are good candidates for immobilizing and delivering larger biomolecules (Varga et al., 2021).

The ion-exchange performance of LDH is affected mainly by the potential difference between the interlayer anions and the environmental anions, and the larger the difference, the better the exchange performance of LDH. For different erosive environmental ions, the interlayer anions of LDH should be selected specifically (Wu et al., 2019). Owing to the adjustability of its layered structure (Chen et al., 2014) and exchangeability of interlayer ions, LDH is a promising adsorption material (Das et al., 2007; Guo et al., 2009). When LDH is used as a supplementary cementitious material for marine concrete, it can adsorb corrosive anions through anion exchange and enhance corrosion resistance (Chen et al., 2021; Mir et al., 2021; Wang et al., 2021).

The corrosion resistance of LDH will be compromised if the corrosive anions combine with heavy metal ions from the environment and form an electropositive complex. Hence, the problem caused by heavy metal ions can be solved by coating negatively charged calcium-based Mnt (Ca-Mnt) on the surface of LDH sheets to construct the required composite material (Bakr et al., 2018). Two-dimensional layered materials (e.g. Mnt and LDH) are the most widely chosen additives to improve the properties of organic-inorganic composites due to the abundant hydroxyl groups on the surfaces. The surface hydroxyl groups are used to construct a hydrogen-bond network between the hydroxide layers and the organic guests, facilitating the fabrication of various functional organic-inorganic composites (Tian et al., 2018). In the case of LDH, the exchange between interlayer anions and chloride ions is facilitated only when the affinity between interlayer anions and lamellae is lower than the affinity between lamellae and chloride ions. Owing to the low affinity of chloride ions, the selection of the corrosion inhibitor anion is greatly restricted. According to the previous literature (Miyata, 1983; Roobottom et al., 1999; Wu et al., 2019), nitrate ions render a smaller affinity than chloride ions. LDH, loaded with nitrate (NO_3-LDH), is a promising candidate to be an inhibitor of chloride ion corrosion.

On the basis of LDH-assisted anion regulation, the negative charge characteristic of Mnt was used to regulate the above-mentioned heavy metal ions. While adsorbing the corrosion anions, calcium ions were replaced between Mnt layers and nitrate ions were replaced between LDH layers during the process of curing corrosive substances, producing calcium nitrate and forming a passive film on the surface of the reinforced concrete and thereby increasing its durability. The objective of the present study was to combine the characteristics of LHD and Mnt to construct and characterize an LDH/Mnt composite as a corrosion-resistant inhibitor for concrete, with an eye toward finding a solution to the problem of corrosion of marine concrete.

Materials and Methods

Materials

All chemicals used in this work were of analytical grade and used without further purification. Magnesium nitrate hexahydrate was obtained from BeiLian

https://doi.org/10.1007/s42860-023-00252-6 Published online by Cambridge University Press

Chemical Co., Ltd (Tianjin, China). Aluminum nitrate nonahydrate and sodium chloride were purchased from ZhiYuan Chemical Co., Ltd (Tianjin, China). Sodium hydroxide was supplied by AoPu Chemical Co., Ltd (Wuhan, China). Anhydrous sodium sulfate was brought from RuiJinTe Chemical Co., Ltd (Tianjin, China). Ca-Mnt was provided by TianYu Bentonite Technology Co., Ltd (Shanghai, China), separating from the bentonite by centrifugation with a maximum moisture content of 2% and a CEC of 0.93 meq/g. The chemical composition of Ca-Mnt was supplied by the producer TianYu Bentonite Technology Co., Ltd (Tianjin, China) (Table 1). Carbon dioxide-free water was used in the aqueous solutions and in filtration.

Synthesis

Synthesis of Mg-Al-NO_3 LDH

The co-precipitation method was adopted to prepare NO_3-LDH because it exhibited a high anionic intercalation rate due to the stable partial structure among various preparation methods for LDH (Zuo et al., 2019). Mg-Al-NO_3 LDH was prepared by the co-precipitation method also. Solution A with 0.03 mol of magnesium nitrate and 0.015 mol of aluminum nitrate in 50 mL of carbon dioxide-free water and solution B with 0.09 mol of sodium hydroxide in 50 mL of carbon dioxide free water were dropped simultaneously into a 150 mL three-necked flask using a 60 mL constant-pressure separatory funnel under vigorous stirring and N_2 atmosphere. After the resulting suspension was stirred for 24 h at 500 rpm, the slurry was allowed to stand undisturbed until crystallization occurred, then it was filtered and washed using carbon dioxide-free water. The filter cake was dried for 24 h and ground into a powder.

Synthesis of LDH/Mnt composite

The self-assembly of LDH and Mnt, with dissimilar layer charges, was carried out by the peeling and assembling processes (Tonda et al., 2018). The resulting LDH was mixed with Ca-Mnt in mass ratios of LDH/Mnt = 1:0.33, 1:0.5, 1:1, 1:2, and 1:3. The value of the Mnt in the mass ratio was taken as the label, e.g. LDH/Mnt-0.33 is the compound with a mass ratio of LDH:Mnt = 1:0.33; LDH/Mnt-0.5 is the label for LDH:Mnt = 1:0.5, etc.

The powder mixture was added to a 500 mL flask and 200 mL of carbon dioxide-free water was added to the flask. The suspension was stirred for 24 h. After the layers of LDH and Mnt were peeled, it was placed in an ultrasonic cleaner and sonicated at 80°C for 5 h. The ultrasonic solution was centrifuged for 5 min at 2248 g. The filter cake was dried for 24 h and ground into powder. The particle size of the LDH/Mnt composite inhibitor is shown in Table 2.

Table 2 The characteristic surface properties of LDH, Mnt, and LDH/Mnt composites

Materials	Specific surface area (m^2/g)	Pore diameter, *D* (nm)	Pore volume, *V* (cm^3/g)
Mnt	63.40	8.65	0.14
LDH	89.64	27.40	0.63
LDH/Mnt-0.33	79.25	26.08	0.50
LDH/Mnt-0.5	76.69	23.50	0.48
LDH/Mnt-1	88.10	14.02	0.33
LDH/Mnt-2	66.96	14.08	0.25
LDH/Mnt-3	58.47	16.65	0.25

Characterization

X-ray diffraction (XRD) measurement

The structures of synthesized LDH and five LDH/Mnt composite materials were characterized by XRD analysis. The patterns were collected using a Bruker D8 Advance powder X-ray diffractometer (Bruker Co., Bremen, Germany) equipped with a CuKa radiation source (λ = 1.5406 Å; 40 kV, 30 mA) from 3 to 70°2θ at a scanning rate of 5°2θ/min.

Table 1 Elemental analysis of the raw Ca-Mnt

	Oxide content (mass %)							
	SiO_2	Al_2O_3	Fe_2O_3	FeO	MgO	CaO	Na_2O	K_2O
Ca-Mnt	65.2–78.2	12.6–15.7	2.0–3.0	1.7	2.5	4.10	2.45	0.6

https://doi.org/10.1007/s42860-023-00252-6 Published online by Cambridge University Press

Laser Raman spectroscopy measurement

The laser Raman spectra were recorded using an Horiba JY LabRAM HR Evolution instrument (Horiba Co., Kyoto, Japan). Raman scattering was excited by a frequency-doubled Nd:YAG laser at a wavelength of 532 nm with an incident power of the laser on the sample of ~50 mW. The sample was scanned three times for 20 s. The laser beam was focused on individual particles using a 100 ×/0.50 NA microscope objective. For the calibration procedure, the peak level of 520.7 nm was calibrated with a silicon wafer.

N_2-adsorption/desorption measurement

In order to confirm the pore-size distribution and the surface areas of synthesized LDH and LDH/Mnt composite materials, N_2 adsorption-desorption isotherms were determined at 77 K using a Micromeritics ASAP 2460 instrument (Micromeritics Co., Norcross, Georgia, USA). Degasification of samples was performed before measurements for 12 h at 100℃ under vacuum (10–5 mm Hg).

Transmission electron microscope (TEM) measurements

The morphologies of synthesized LDH and composite materials were examined using an FEI Tecnai G2 F20 S-Twin 200 kV field emission transmission electron microscope (FEI Co, Hillsboro, Oregon, USA). The powder samples were placed in an ethanol solution and dispersed ultrasonically for 20 min. The droplets were then dropped onto the copper film to prepare the sample for testing.

Thermo-gravimetric analysis and differential scanning calorimetry (TG-DSC) measurement

The TG-DSC analyses of LDH/Mnt composite materials were performed using a STA499F3 Jupiter synchronous thermal analyzer (Netzsch Co., Selb, Germany), heating from room temperature to 800℃ at a heating rate of 10℃/min in a nitrogen protected atmosphere to ensure that mass loss was not affected by air moisture.

X-ray fluorescence (XRF) measurement

The elemental contents of the composite materials LDH/Mnt-1 were determined using an S2RANGER energy dispersive X-ray fluorescence (XRF) spectrometer (Bruker AXS Co., GmbH, Karlsruhe, Germany), with grinding and pressing of the randomly oriented sample powders to ensure uniform density and smooth surface.

Equilibrium Isotherm of LDH/Mnt Composites

A series of sodium chloride and sodium sulfate solutions with various concentrations (100, 200, 500, 800, 1000, 2500, and 5000 mg/L) was added to 0.3 g of the composite sample (LDH/Mnt-1) and stirred at room temperature for 6 h to achieve adsorption equilibrium. The centrifugation was carried out at 2248 x *g* for 5 min. The supernatant was filtered through a 0.22 μm porous membrane. The concentrations of chloride, sulfate, nitrate, and calcium ions in the solution were determined by ion chromatography (LC-20, Shimadzu Co., Kyoto, Japan). The test was repeated three times, and after data processing, the chloride and sulfate adsorption equilibria were obtained. The loading capacity of LDH for chloride was calculated using the following equation:

$$q_e = \frac{(C_0 - C_e)V}{m} \quad (1)$$

where q_e is the adsorptive capacity of LDH/Mnt composite at equilibrium (mg/g), V is the volume of solution (L), C_0 and C_e are the initial and equilibrium concentrations of chloride (mg/L), and m is the weight of LDH (g).

The Langmuir and Freundlich models were used to fit the equilibrium isotherm experimental data to reflect the corrosion resistance of LDH/Mnt composites. The Langmuir model is based on the solute monolayer adsorption and assumes that the surface of the adsorbent is uniform. Hence, the interactions between adsorbed particles are ignored. The adsorption formula is as follows:

$$q_e = \frac{Q K_L C_e}{1 + K_L C_e} \quad (2)$$

https://doi.org/10.1007/s42860-023-00252-6 Published online by Cambridge University Press

where Q is the maximum adsorption capacity (mg/g) of chloride ions and sulfate ions under monolayer covering, K_L is the related Langmuir constant (L/mg), and C_e is the equilibrium concentration (mg/L) of chloride or sulfate in aqueous solution (Ai et al., 2011; Xu et al., 2017). The Freundlich model is used as an empirical formula to describe adsorption behavior on an heterogeneous surface, and its equation is expressed as follows (Lv et al., 2006):

$$q_e = K_F C_e^n \quad (3)$$

where K_F and n are Freundlich constants related to temperature. The value of n reflects the linearity of Freundlich model.

Corrosion Resistance Analysis of LDH/Mnt Composites on Carbon Steel in SSCP Solution

Electrochemical measurement

In order to simulate the permeability of chloride and diffusion of carbon dioxide in the concrete pores, the current work applied the simulated concrete carbonated pore (SCCP) solution with the following preparation method: an excess amount of calcium hydroxide (5 g) was added to deionized water (500 mL) and the saturated calcium hydroxide solution was obtained after precipitation for 24 h. An appropriate amount of 3 wt.% sodium bicarbonate solution was used to adjust the pH to 11.0 and the filtrate was the SCCP solution.

A three-electrode setup was used in electrochemical analysis. The working electrode was carbon steel with a size of Φ8 mm×10 mm, the reference electrode was a saturated calomel electrode (SCE), and the counter electrode was a platinum sheet. Carbon steel was polished with ~400–2000 grade sandpaper and cleaned ultrasonically with acetone before the tests. One end of the working electrode was connected to a copper wire, and the other parts were sealed with epoxy resin except for the working surface of 0.5 cm^2. Sodium chloride of 0.3 mol/L, close to the sea water chlorinity of 20,000 ppm, was added to the SCCP solution to simulate chloride contaminations. Five types of LDH/Mnt composites were added at a concentration of 15 g/L.

The electrochemical measurements were carried out using a CH1760E electrochemical workstation at room temperature. The electrochemical impedance spectroscopy (EIS) was performed at the open-circuit potential (OCP) with a stable open-circuit potential. The vibration frequency was 100 Hz and the AC amplitude was 10 mV. After repeating the test three times and averaging, the EIS data were analyzed using the *ZView* 3.1 software (Zuo et al., 2019).

Fourier-transform infrared spectroscopy (FTIR) measurements

After the equilibrium isotherm experiment, sodium chloride and sodium sulfate, with initial concentrations of 500 mg/L and 5000 mg/L, respectively, were selected for comparison. The solid-liquid mixture was centrifuged and dried; FTIR spectroscopy (Nicolet iS5 FTIR spectrometer (Thermo Fisher Scientific Co., Waltham, Massachusetts, USA)) was used to analyze the changes in functional groups after ion exchange of composite materials. The samples were embedded in KBr disks (at a 100:1 KBr:sample ratio) and the transmittance spectra were recorded over the frequency range 4000–400 cm^{-1} and a resolution of 4 cm^{-1}.

Analysis of the formation of passive film

In order to investigate the effect of LDH/Mnt composites on the formation of a surface passive film, a steel bar (φ 8 mm×10 mm) was placed in 100 mL of SCCP solution and sodium chloride was added to it. The concentration of LDH/Mnt-1 was 1 g/L. A solid material was generated on the surface of the steel bar by using the bar to stir the SCCP solution continuously. The surface products (passive film) after anionic erosion were tested using the aforementioned FEI-TEM instrument and a Thermo Fisher Scientific K-Alpha XPS instrument (Thermo Fisher Scientific Co., Waltham, Massachusetts, USA). With an AlKα radiation source, the test energy was 1486.8 eV, the test spot area was 30–500 μm, the test tube voltage was 15 kV, and the tube current 10 mA. The background vacuum in the sample chamber was 2×10^{-9} mbar, and the presence or absence of iron, calcium, and oxygen in the samples was noted.

https://doi.org/10.1007/s42860-023-00252-6 Published online by Cambridge University Press

Results and Discussion

Characterization

XRD analysis

The XRD patterns of NO_3-LDH (Fig. 1) exhibited the characteristic reflection peaks of LDH at 11.52 and 23.40°2θ, corresponding to the (003) and (006) reflection planes, respectively (Gomes et al., 2020). According to Bragg's equation, the d_{003} spacing of LDH was calculated to be 0.7629 nm, which is in good agreement with previous reports (0.78 nm, Zhang et al., 2017). The characteristic reflection peaks of LDH and the characteristic (001) reflection peak of Mnt (d_{001} = 1.46 nm) were observed in all composites, and the degree of crystallinity could be seen from the sharpness of the reflection peaks; it changed with different mass ratios of LDH/Mnt. When the mass ratio of LDH/Mnt was 1:1 or 1:2, the composite crystallized well. Both LDH and Mnt remained in their crystalline states in all composites. Compared with the XRD patterns of LDH and Mnt alone, the lesser intensity of the composites was caused by the mixture of the two. The position of the characteristic reflection peak of LDH shifted to the left (to ~10.82°2θ) in the synthesized intercalated composite, indicating that the interplanar spacing of the LDH/Mnt composites increases due to the self-assembly of LDH and Mnt (Bakr et al., 2016). In addition, the characteristic peak of LDH/Mnt-1 (~21.65°2θ) corresponded to the later analysis of TEM images. The composition of LDH and Mnt was not a regular layer-by-layer assembly but a random assembly. However, the LDH/Mnt composites in the present work were used mainly to provide their interlayer ions, so random assembly of layers had no effect on the ion-exchange property.

Laser Raman spectroscopy analysis

In the Raman spectrum of LDH (Fig. 2), the characteristic peak of nitrate in the triclinic system occurred at 1048 cm^{-1}, while in the composites, the characteristic peak of nitrate in the rhombic crystal system at 1066 cm^{-1} could be seen (Jentzsch et al., 2013), indicating that NO_3-LDH was prepared successfully. In the Raman spectrum of Mnt, the strongest bands occurred at 147 cm^{-1}, which was also reflected in all the composite material samples. The occurrence of this characteristic peak was attributed to the vibrations of the distorted MO_6 octahedron with S_6 symmetry where M is the octahedral cation (Frost & Rintoul, 1996). Other weaker bands were observed at 262 and 702 cm^{-1}. The former is attributed to the vibrations of the H–O–H triangle of C_{2V} symmetry and the latter to the $\nu_1(a_1)$ mode of the SiO_4 tetrahedra (Vaculíková et al., 2019).

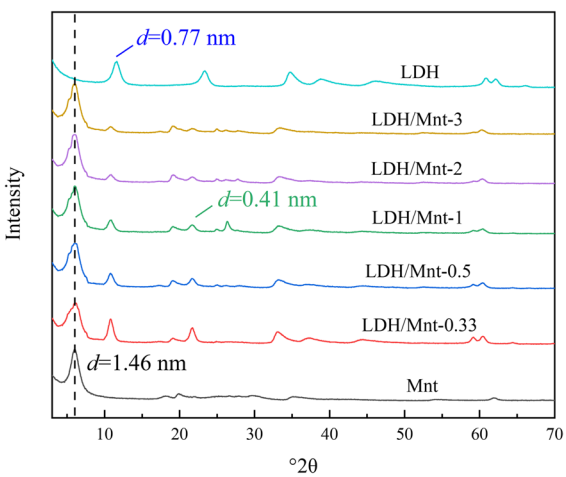

Fig. 1 XRD patterns of LDH, Mnt, and LDH/Mnt composite materials with various mass ratios of Mnt (LDH/Mnt-0.33, LDH/Mnt-0.5, LDH/Mnt-1, LDH/Mnt-2, LDH/Mnt-3)

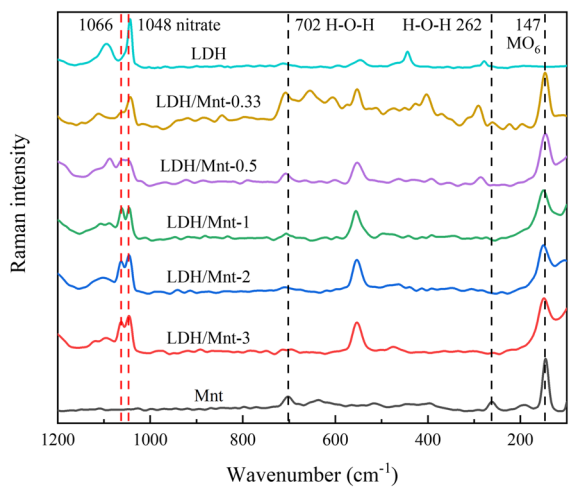

Fig. 2 Laser Raman spectra of LDH, Mnt, and LDH/Mnt composite materials

https://doi.org/10.1007/s42860-023-00252-6 Published online by Cambridge University Press

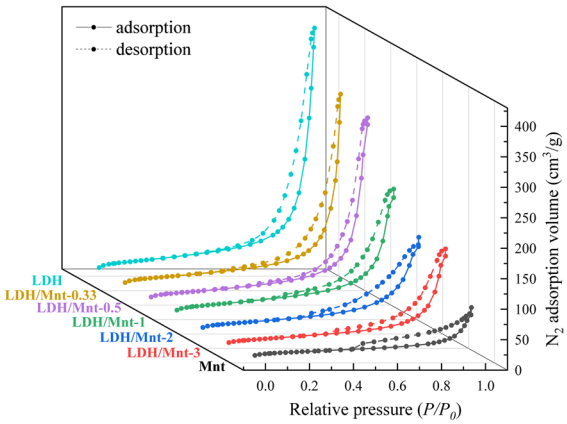

Fig. 3 N_2-adsorption/desorption isotherms of NO_3-LDH, Mnt, and LDH/Mnt composite materials

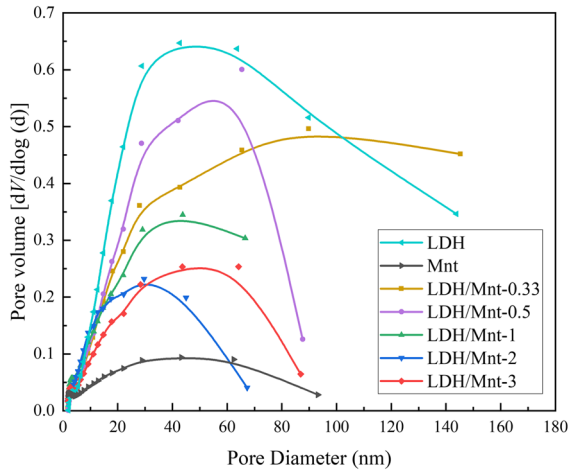

Fig. 4 Barrett-Joyner-Halenda pore-size distributions for NO_3-LDH, Mnt, and LDH/Mnt composite materials

N_2-adsorption/desorption analysis

The N_2-adsorption/desorption isotherms of the NO_3-LDH, Mnt, and LDH/Mnt composites (Fig. 3) revealed that all the samples belonged to type IV adsorption according to the IUPAC classification, which meant the NO_3-LDH, Mnt, and LDH/Mnt composites belonged to a mesoporous-type material characterized by a H_3-type hysteresis loop (Sing, 1985, 1989). The mesoporous type indicated the presence of aggregates of plate-like particles giving rise to slit-shaped pores with non-uniform size and shape (Lecloux & Pirard, 1979). The isotherm showed that the more LDH components in the composite, the larger the pore volume and BET specific surface area. The pore-size distribution of the NO_3-LDH, Mnt, and LDH/Mnt composites were calculated from Barrett-Joyner-Halenda (BJH) methods (Fig. 4). The BJH pore-size is calculated as follows:

$$V=\frac{4}{3}\pi r^3 N/\mathrm{A}v \tag{4}$$

where V is the pore volume, r is the pore size, N is the number of adsorbent molecules, A is Avogadro constant, and v is the molecular volume of adsorbent. Due to the large range of pore-size distribution, logarithmic coordinates were used for analysis, where dV/dlog(d) represented the pore volume. The surface areas of the NO_3-LDH, Mnt, and LDH/Mnt composites were calculated from Brunauer-Emmett-Teller (BET) methods (Table. 2). The data obtained from BJH indicated that the mean pore size of the samples was fitted well to the size range of layered materials and revealed that the pore-size distribution of the LDH was much wider than that of Mnt. However, these large pores disappeared, and the pores were highly uniform after formation of the composite.

TEM analysis

The microstructure of synthesized LDH and LDH/Mnt-1 composite (Fig. 5) revealed that LDH possesses a polygonal lamellar structure (Fig. 5a). The lamellar size was relatively uniform, compact stacking was irregular, and intergranular spacing was small, because of preparation under a saturated sodium hydroxide solution, where LDH nucleated rapidly and particles grew rapidly. Meanwhile, some LDH lamellae grew crosswise under the condition of weak interactions, forming support structures to improve agglomeration, which was conducive to the stability of layered structures (Adachi-Pagano et al., 2003). In Fig. 5b with greater magnification, the lattice fringe spacing of LDH was determined to be 0.21 nm, corresponding to the peak position (006) in the XRD pattern. After composite formation, the lamellar structure of Mnt and LDH flakes were observed (Fig. 5c) on the surface and the interlayer structure became loose and dispersed due to the self-assembly of LDH and Mnt layers (Dong et al., 2013). The lattice fringe spacing (0.41 nm) of the new layer structure occurred in the image of the composite

https://doi.org/10.1007/s42860-023-00252-6 Published online by Cambridge University Press

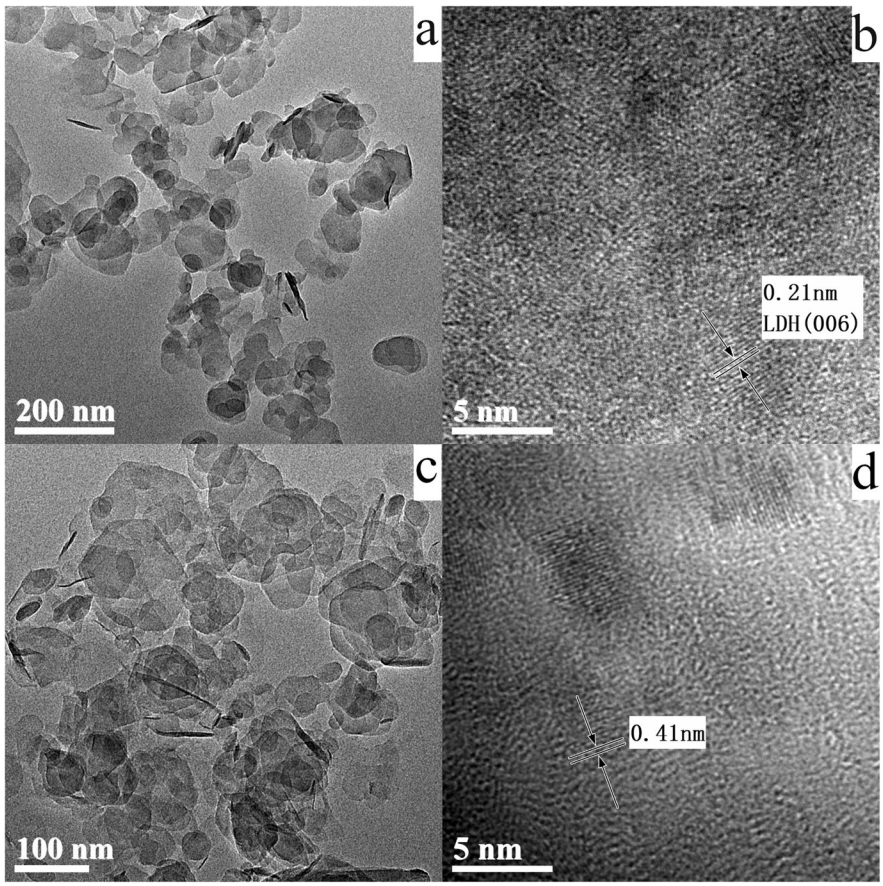

Fig. 5 TEM images of **a**,**b** LDH and **c**,**d** LDH/Mnt-1

sample LDH/Mnt-1 (Fig. 5d), corresponding to the characteristic peak of LDH/Mnt-1 (21.65°2θ) in the XRD pattern.

TG-DSC analysis

The combined thermogravimetry and differential scanning calorimetry behavior of LDH/Mnt composites were investigated by TG-DSC tests (Fig. 6). Two important weight-loss stages appeared on the TG curves of all samples (Fig. 6a). The mass decline in the first stage was caused mainly by the desorption of surface-adsorbed water and loss of interlayer bound water, corresponding to the wide endothermic valley at ~200℃ on the DSC curve (Fig. 6b), which was consistent with the commonly known thermal characteristics of LDH (Kanezaki, 1998). According to the calculation, the mass loss of five groups of samples during the first stage was ~10%. Among them were two small thermal valleys in the TG curve of LDH/Mnt-3, i.e. at 210 and 144°C, representing the thermal characteristics of Mnt (Lv et al., 2015) and corresponding to the removal of interlayer water and adsorbed water. When the proportion of LDH in the composite increased, the proportion of Mnt decreased and the small endothermic peak near 144°C decreased gradually and finally disappeared. In the second weight-loss stage, mainly at ~240–480°C, the hydroxyl groups were removed from the hydroxide layer of the LDH, along with removal of the intercalated nitrate ions. The mass loss of LDH/Mnt-0.33, LDH/Mnt-0.5, LDH/Mnt-1, LDH/Mnt-2, and LDH/Mnt-3 during the second stage was 17, 12, 11, 8, and 5.53%, respectively. When the proportion of LDH in the complex increased, the mass loss during the second stage also increased due to the decomposition of nitrate ions. The mass

https://doi.org/10.1007/s42860-023-00252-6 Published online by Cambridge University Press

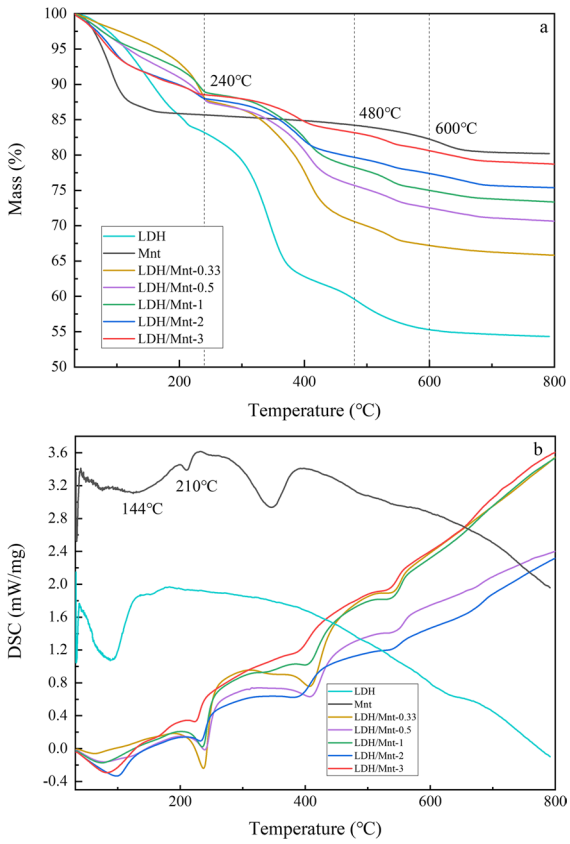

Fig. 6 **a** TG curve and **b** DSC curve of NO_3-LDH, Mnt and LDH/Mnt composite materials

proportion of LDH was calculated as 74.12, 62.11, 46.13, 32.92, and 22.84%, respectively, which is consistent with the theoretical proportion. Moreover, the removal of hydroxyl groups from Mnt lamellae generally occurs in the temperature range of 600–700°C, showing slight fluctuations in the curve (Zou et al., 2020). At >600°C, the residual nitrate ions between the layers of NO_3-LDH continued to decompose and $MgAl_2O_4$ started to crystallize (Wu et al., 2019). At ~800–953°C, the structure of Mnt disintegrated, the lattice was completely destroyed, and an amorphous structure was formed.

XRF analysis

According to previous literature (Yusuf et al., 2021), the structural formula of LDH is $Mg_{1-x}^{2+}Al_x^{3+}(OH)_2(NO_3^-)_x{\cdot}mH_2O$ and the structural formula of Mnt is $E_x(Al_{2-x},Mg_x)_2{\cdot}\{p[Si_4O_{10}]\}(OH)_2{\cdot}4H_2O$. The observed fractions of Mg and Al in the octahedral sheet were Mg/(Mg+Al) = 83.60% and Al/(Mg+Al) = 16.40% (Table 3). Plugging the ratio into the structural formula for LDH and Mnt resulted in x=0.328, so the stoichiometries of Mg and Al in 100g LDH/Mnt-1 in the Mnt structural formula were, therefore, 1.672 and 0.328 mol, respectively. Based on the mass ratio of Fe_2O_3, CaO, Na_2O and K_2O and their relative molecular mass, The exchangable cation content, E_x(Fe, Ca, Na, K), was a total of 0.0652 mol in 100g LDH/Mnt-1. As E_x was supplied entirely by Mnt, the amount of Mnt was 0.39 mol. The relative fraction of Si in the Mnt, *p,* was calculated from the stoichiometry of Si and based on the amount of Mnt, resulting in a value of 2.37. After the removal of Mg and Al from Mnt, the amounts of Mg and Al in the complex were 0.2576 and 0.051 mol, respectively. According to the proportions, Mg/(Mg+Al) = 83.47% and Al/(Mg+Al) = 16.53%, therefore, the amounts of Mg and Al in the structural formula of LDH were 0.836 and 0.164 mol, respectively, where the amount of LDH was calculated to be 0.31 mol. *m* generally decreased with increase in *x*, showing a relationship of $m = 0.8 - x$. Hence, $m = 0.636$ in LDH/Mnt-1. Therefore, the molar ratio of LDH/Mnt-1 was 0.31/0.39. The formula of NO_3-LDH was $Mg_{0.836}^{2+}Al_{0.164}^{3+}(OH)_2(NO_3^-)_{0.164}{\cdot}0.636H_2O$ and the formula of Mnt was $(Fe,Ca,Na,K)_{1.672}(Al_{0.328},Mg_{1.672})_2{\cdot}\{2.37[Si_4O_{10}]\}(OH)_2{\cdot}4H_2O$.

Equilibrium Isotherm of LDH/Mnt Composites

LDH/Mnt-1 was selected for adsorption experiments. The adsorption characteristics and mechanism of LDH/Mnt-1 on corrosive ions under various environmental conditions were investigated, and the equilibrium results from ion chromatography were plotted

Table 3 Elemental analysis of LDH/Mnt-1

Element	Si	Mg	Al	Fe	Ca	Na	K
Mass (g)	39.62	26.10	25.91	3.61	2.18	1.40	0.70
%	39.81	26.23	26.03	3.63	2.19	1.41	0.70

https://doi.org/10.1007/s42860-023-00252-6 Published online by Cambridge University Press

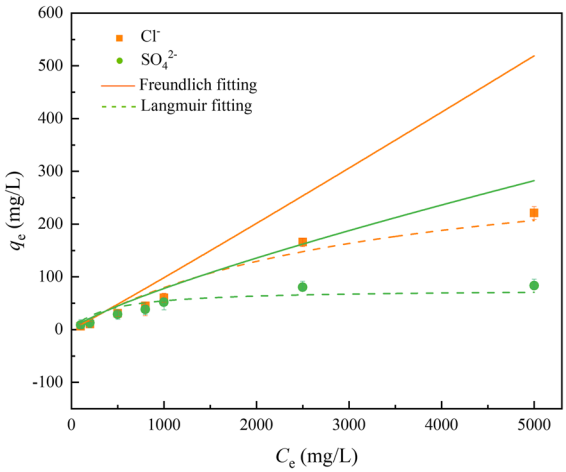

Fig. 7 Equilibrium isotherms of chloride and sulfate adsorption on LDH/Mnt-1

(Fig. 7, Table 4). The maximum adsorption capacity with respect to chloride and sulfate ions, according to the Langmuir model, was 206.89 and 79.69 mg/L, respectively. These values are greater than the value of 50 mg/L reported previously for both (Cao et al., 2017).

The parameters of the Langmuir and Freundlich equations (Table 5) revealed the adsorption behavior of chloride and sulfate ions on LDH/Mnt-1 and the mechanism of solute–surface interaction. The correlation coefficients of Langmuir isotherms and Freundlich isotherms were 0.9998 and 0.9997, indicating that the correlation coefficient between the two was close. According to the fitting curve in Fig. 7, it was considered that Langmuir isotherms fitted more closely with the experimental data and were consistent with the data reported from other studies (Javadian et al., 2013; Xu et al., 2017). This may be due to the fact that LDH interlayer ions are connected to the lamellae by weak hydrogen bonds; because of the positive charge remaining in the host layer, anions were adsorbed into the interlayer to maintain electrical neutrality. Therefore, only one ion could be immobilized per adsorption site, which was equal to the adsorption which occurred on a homogeneous surface. The nonlinear coefficient (n) of the Freundlich model ranged from 0.5 to 2 during chloride (n = 1.0331) and sulfate (n = 0.7994) adsorption, respectively, which was relatively small and indicated that adsorption occured easily.

(level2)Corrosion Resistance Mechanism of LDH/Mnt Composites on Carbon Steel in SSCP solution

Electrochemical analysis

EIS was carried out to explore the corrosion resistance behavior and mechanism of the self-assembled LDH/Mnt composites, including the Nyquist and Bode plots of carbon steel soaked in SCCP solution with and without LDH/Mnt composites (Fig. 8). The fitting parameters are summarized in Table 6.

The impedance spectrum of the control solution (Fig. 8a) consisted of a small, high-frequency capacitive ring and a low-frequency Warburg impedance, indicating corrosion of the carbon steel surface. After the addition of the LDH/Mnt composite, the Warburg impedance disappeared from the Nyquist plots and only the capacitive ring remained visible. The diameter of the capacitive ring increased significantly and the maximum phase angle became larger and wider, indicating that the LDH/Mnt composite greatly

Table 4 Anion concentrations of LDH/Mnt-1 after stirring in the solution of chloride and sulfate

Initial anion concentrations (mg/L)	NaCl environment			Na_2SO_4 environment			Initial concentrations error (mg/L)
	Cl^- (mg/L)	NO_3^- (mg/L)	Ca^{2+} (mg/L)	SO_4^2 (mg/L)	NO_3^- (mg/L)	Ca^{2+} (mg/L)	
100	6.39	0.06	46.57	8.72	0.11	5.99	0.27
200	10.76	0.24	8.72	12.92	0.15	7.84	0.31
500	31.00	0.21	8.78	29.20	0.12	8.95	0.25
800	44.99	0.28	9.20	38.42	0.19	12.69	0.38
1000	60.34	0.21	8.54	52.09	0.13	10.41	0.26
2500	166.02	0.34	11.12	80.37	0.27	17.83	0.45
5000	221.14	0.36	14.71	83.24	0.28	28.16	0.61

https://doi.org/10.1007/s42860-023-00252-6 Published online by Cambridge University Press

Table 5 Langmuir and Freundlich parameters for the chloride and sulfate adsorption isotherms of LDH/Mnt-1

Model	Langmuir			Freundlich		
LDH/Mnt-1	Q (mg/g)	K_L (L/mg)	R^2	K_F	n	R^2
Cl^-	344.83	0.0003	0.9998	0.0783	1.0331	0.4977
SO_4^{2-}	76.36	0.0025	0.9997	0.3117	0.7994	0.5141

improved the impedance of carbon steel. The occurrence of disposable time constants (only one capacitive reactance arc) in the Bode diagram (Fig. 8b) was attributed to the formation of a passive film on the surface of carbon steel (Wang et al., 2014). At this time, the high polarization resistance in the SCCP solution indicated that the carbon steel electrode was completely passivated. The diameter of the capacitive ring followed the order: LDH/Mnt-2 > LDH/Mnt-1 > LDH/Mnt-0.5 > LDH/Mnt-3 > LDH/Mnt-0.33, which was consistent with the trend of corrosion resistance. LDH/Mnt-1 and LDH/Mnt-2 rendered the optimal corrosion resistance, protecting the steel bar from corrosion caused by chloride ions.

To demonstrate the desirable correspondence between elements of a circuit and physical processes (David & Driessche, 2011), the electrochemically equivalent circuits (Fig. 9) were used to fit the EIS data, where R_s represents the ohm resistance between the working electrode and the reference electrode, R_{ct} denotes the interfacial charge conversion resistance, and W denotes the Warburg impedance. The total resistance of the circuit can be expressed as the following formula (Javadian et al., 2013):

$$Z = R_S + \frac{R_{ct} + W}{1+(j\omega)Z_{CPE}W+(j\omega)Z_{CPE}R_{ct}} \quad (5)$$

Due to charge transfer, R_{ct} is an important parameter to judge the impedance of the carbon steel. The higher value of R_{ct} corresponded to the greater impedance. The constant phase element (CPE) was used widely to explain the deviation caused by the surface roughness, and its impedance can be expressed as the following formula (Javadian et al., 2013; Ryu et al., 2017):

$$Z_{CPE} = \left[Y_0(j\omega)^u\right]^{-1} \quad (6)$$

where Y_0 represents the size of CPE, the angular frequency, for $j^2 = -1$, j is an imaginary number, and u is the index of CPE. The value of u is related to the uniformity of the carbon steel surface, and the larger the value of u, the better the uniformity. The behavior of CPE depends on the value of index u, and the modified C_{dl} for its actual capacity value is calculated as follows:

$$C_{dl}=Y_0\left(\omega_{max}\right)^{u-1} \quad (7)$$

where ω_{max} is the frequency at which the imaginary part of impedance (Z_{im}) maintains its maximum

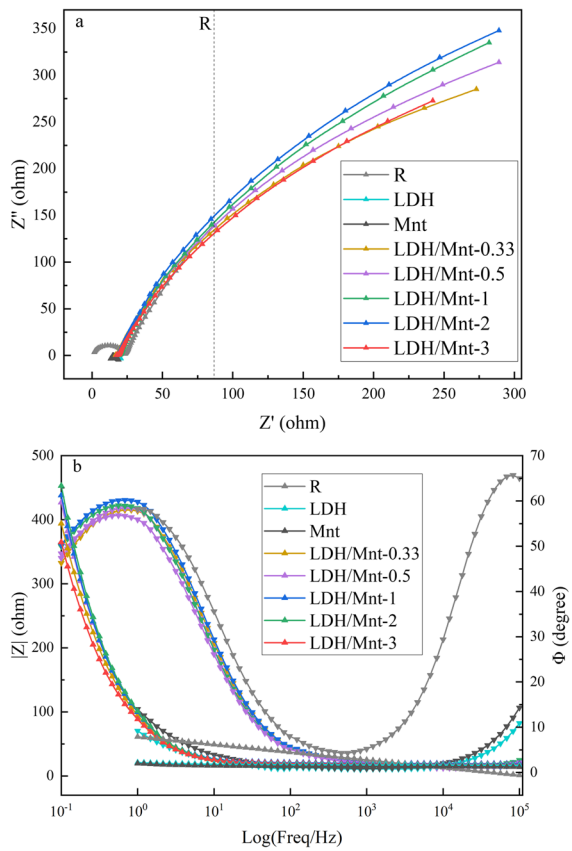

Fig. 8 The **a** Nyquist plots and **b** Bode plots of carbon steel soaked in SCCP solution with and without NO_3-LDH, Mnt, and LDH/Mnt composite materials added after immersion

https://doi.org/10.1007/s42860-023-00252-6 Published online by Cambridge University Press

Table 6 The fitting parameters obtained from EIS with various LDH/Mnt composite materials in SCCP solution

Samples	R_s ($W\ cm^2$)	CPE		R_{ct} ($W{\cdot}cm^2$)	%
		Y_0 ($10^{-5}\ S{\cdot}cm^{-2}s^u$)	u		
R (control group)	20.78	138.20	0.7755	71.53	-
LDH	16.93	422.50	1.0219	959.65	92.55
Mnt	14.57	688.39	0.4979	221.00	67.63
LDH/Mnt-0.33	17.35	274.50	0.7995	948.10	92.46
LDH/Mnt-0.5	19.21	259.61	0.8047	1053.84	93.21
LDH/Mnt-1	19.34	262.75	0.8014	1224.04	94.16
LDH/Mnt-2	17.95	252.96	0.8060	1269.24	94.36
LDH/Mnt-3	18.10	309.67	0.7826	1039.45	93.12

value. Corrosion inhibition efficiency, η%, is calculated according to the following formula (Cao et al., 2017; Javadian et al., 2017):

$$\eta\% = \frac{R_{ct} - R_0}{R_{ct}} \times 100\% \quad (8)$$

In the formula, R_{ct} and R_0 represent the interface charge conversion resistance of carbon steel in SCCP solution before and after adding the composite, respectively. The R_{ct} reflected the corrosion inhibition effect of the passive film on the carbon steel surface before and after the action of composite material. The larger R_{ct} corresponded to better corrosion resistance and greater corrosion inhibition efficiency (η%).

According to the fitting parameters, the R_{ct} value of the carbon steel electrode increased after the addition of LDH/Mnt composite. The R_{ct} values of LDH/Mnt-1 and LDH/Mnt-2 reached 1224.04 and 1269.24 $W{\cdot}cm^2$, respectively, and the corresponding corrosion inhibition efficiency was found to be 94.16 and 94.36%. The *u* value of LDH/Mnt-2 reached its maximum of 0.8060 and the electrode surface became dense and uniform. Y_0 reached a minimum value of $252.96\times10^{-5}\ S{\cdot}cm^{-2}s^u$. Owing to the addition of composites, LDH released the interlayer anions, and calcium cations were replaced by Mnt. When the passive film on the steel surface was subjected to corrosion, the active adsorption of chloride was generated to form a calcium nitrate passive film, forming an active anti-corrosion system and improving the corrosion resistance. In addition, although the corrosion inhibition efficiency of LDH/Mnt-1 was slightly less than that of LDH/Mnt-2, its nitrate content was also 1% less than that of LDH/Mnt-2 according to the result of TG-DSC, so the overall corrosion inhibition performance of LDH/Mnt-1 was outstanding.

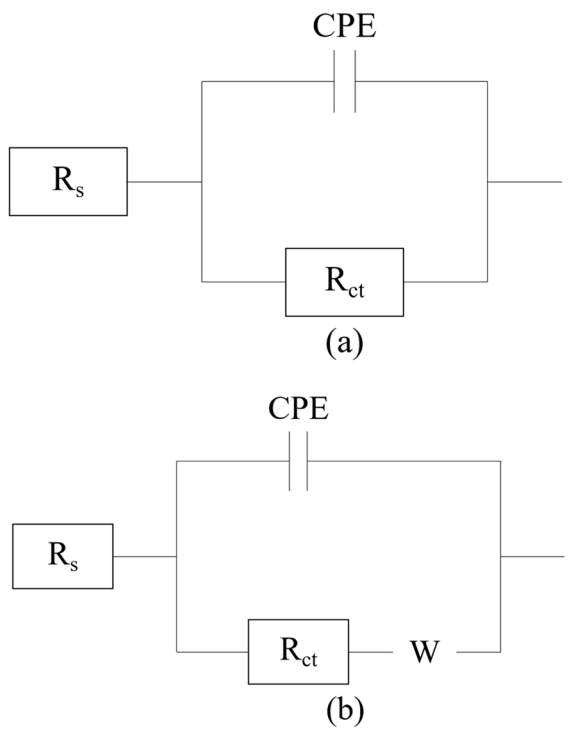

Fig. 9 Electrochemical equivalent circuits used to fit the EIS results in SCCP solution for **a** general semicircle and **b** Warburg type

https://doi.org/10.1007/s42860-023-00252-6 Published online by Cambridge University Press

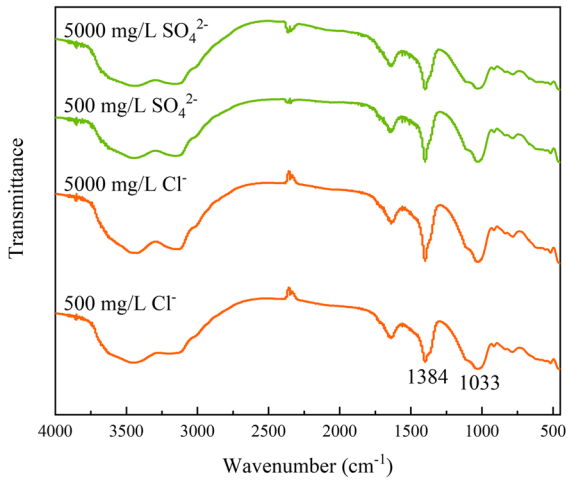

Fig. 10 FTIR spectra of LDH/Mnt-1 after stirring in Cl^- and SO_4^{2-} solutions

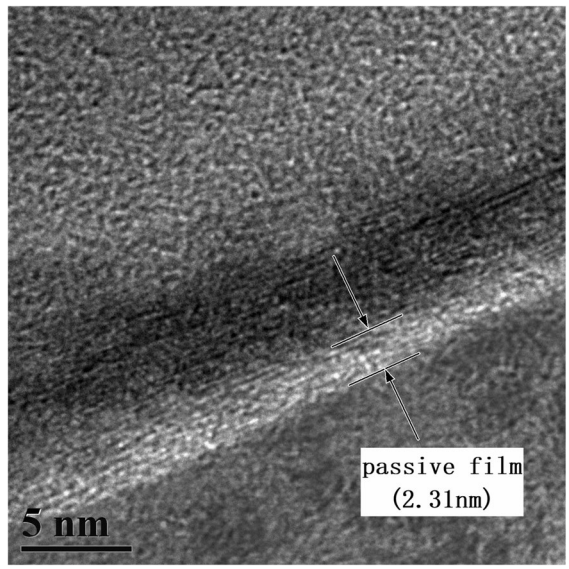

Fig. 11 TEM image of a cross-section of the steel bar after the passive film had formed

FTIR analysis

The FTIR spectra of the precipitates after ion exchange of LDH/Mnt-1 with chloride and sulfate (Fig. 10) demonstrated that the characteristic peaks of the complex sample did not change. However, the intensity of characteristic peaks of nitrate decreased significantly with the increase in adsorbent concentration. The concentration of nitrate ions between LDH layers decreased after the adsorption experiment.

Analysis of the formation of passive film

After the passive film was formed on the surface of the steel bar, three layers were observed in the TEM image of the cross-sectional sample (Fig. 11), including an electron beam, a passive film, and the steel bar (Ohet al., 2014). In particular, the thickness of the second layer or the passive film was ~2.31 nm. The high-resolution X-ray photoelectron spectra (XPS) of Ca 2p and O 1s (Fig. 12a) revealed that the positions located at 351.73 and 348.23 eV correspond to characteristic peaks at Ca $2p_{1/2}$ and Ca $2p_{3/2}$, respectively (Haber et al., 1976; Christie et al., 1983). The O 1s peak in the high-resolution XPS spectra (Fig. 12b) was used to confirm the existence of calcium ions in the form of calcium nitrate. The two dominant O 1s peaks were from calcium nitrate (533.60 eV) and ferric oxide (529.50 eV) (Demri & Muster, 1995). The iron oxide component of the steel bar was mixed in when the surface passivation film was scraped off, but it was not a product of the experiment. The above results showed that the passive film (Fig. 11) generated on the surface is calcium nitrate.

Synthesis Cost

To prepare an LDH/Mnt composite of 1 g, 2.97 g of magnesium nitrate, 2.13 g of aluminum nitrate, 2.40 g of sodium hydroxide, and 1.33 g of Ca-Mnt were required. The cost of the composite per gram was calculated on the basis of prices of the chemicals from corresponding companies (Table 7). The final material cost was ~US$3.32/g. Taking into account the costs of manufacturing and shipment, the overall cost may reach US$60/g, which is comparable with the cost of commercially available inhibitors.

Summary and Conclusions

The LDH/Mnt composites were synthesized successfully by LBL technology for protecting reinforced concrete structures. The XRD patterns revealed that the characteristic peaks of both LDH and Mnt existed in the composites, confirming the presence of both components. Two major stages of weight loss were

https://doi.org/10.1007/s42860-023-00252-6 Published online by Cambridge University Press

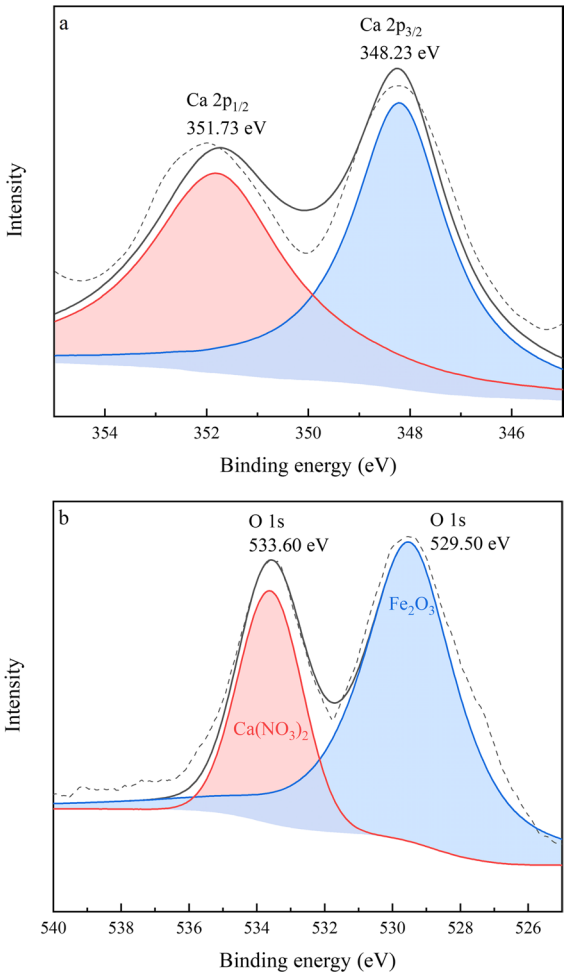

Fig. 12 XPS spectra of the surface product covering the steel bar in SCCP solution with LDH/Mnt-1 after immersion

observed in TG-DSC curves and the weight loss of LDH/Mnt-3 in the second stage was greatest. A preliminary conclusion by the present authors was that LDH/Mnt-3 had the greatest rate of anion intercalation.

Table 7 Cost analysis of the LDH/Mnt composite prepared with the unit price of the raw materials used

Raw materials	Unit price (US$/g)	Material required (g)	Price (US$/g)
Magnesium nitrate	0.01	2.97	0.03
Aluminum nitrate	0.01	2.13	0.02
Sodium hydroxide	0.01	2.40	0.02
Ca-Mnt	2.44	1.33	3.25
Total	-	-	3.32

Analysis of the equilibrium adsorption isotherms revealed that the Langmuir model was more suitable for the experimental data than the Freundlich model, demonstrating that only one ion can be immobilized per adsorption site, which is equal to the adsorption which occurred on the homogeneous surface. The maximum adsorption capacities of chloride and sulfate ions using the Langmuir isotherm model were 206.89 and 79.69 mg/L. The adsorption capacity is greater than the value quoted in previous literature (both 50 mg/L).

The EIS analysis confirmed that the addition of LDH/Mnt increased the R_{ct} value significantly, and the rust inhibition efficiency values of LDH/Mnt-0.33, LDH/Mnt-0.5, LDH/Mnt-1, LDH/Mnt-2, and LDH/Mnt-3 were 92.46, 93.21, 94.16, 94.36, and 93.12%, respectively. Among them, the rust inhibition efficiency performance of LDH/Mt-3 was poor due to the large Mnt content. The rust inhibition efficiency of conventional measures was generally ~85%, and that of all composites was greater than this. LDH/Mnt-1 rendered the optimal protection effect due to high rust inhibition efficiency. The XPS analysis showed that the LDH/Mnt-1 caused a passive calcium nitrate film to form on the surface of the steel bar.

The LDH/Mnt composite is a very efficient corrosion inhibitor, showing promise in the areas of concrete structures and marine engineering. The chloride ions are adsorbed by LDH and sequestered, whereas nitrate ions are released and combined with calcium ions, which are released by Mnt, to form a passive film. Throughout the process above, the LDH/Mnt composite can control the concentration of anions in seawater and sea sand environments, thus improving the rust inhibition of marine concrete.

Acknowledgments This research was supported jointly by the National Natural Science Foundation of China (42202042), Liaoning Province "Xingliao talent plan project" (XLYC2007105 and XLYC2007176), Natural Science Foundation of Liaoning Province (2021-MS-245), Projects of the Educational Department of Liaoning Province (LJKZ0594), and by the Foundation of Key Laboratory of Clay Mineral Applied Research of Gansu Province (CMAR-2022-02).

Authors' contributions Limei Wu and Ning Tang contributed to the conception of the study; Mingxi Sun performed the experiment and contributed significantly to manuscript preparation; Xiaolong Wang, Yushen Lu, Lili Gao, Qing Wang, and Ling Hu helped to perform the analysis with constructive discussions.

https://doi.org/10.1007/s42860-023-00252-6 Published online by Cambridge University Press

Funding This research was jointly supported by National Natural Science Foundation of China (42202042), Liaoning Province "Xingliao talent plan project" (XLYC2007105 and XLYC2007176), Natural Science Foundation of Liaoning Province (2021-MS-245), Projects of the Educational Department of Liaoning Province (LJKZ0594), Foundation of Key Laboratory of Clay Mineral Applied Research of Gansu Province (CMAR-2022-02).

Data availability All data generated or analyzed during this study are included in this article.

Code availability Not applicable

Declarations

Conflicts of interest/Competing interests On behalf of all authors, the corresponding author states that there is no conflict of interest.

References

Acharya, H., Srivastava, S. K., & Bhowmick, A. K. (2007). Synthesis of partially exfoliated EPDM/LDH nanocomposites by solution intercalation: Structural characterization and properties. *Composites Science and Technology, 67*(13), 2807–2816. https://doi.org/10.1016/j.compscitech.2007.01.030

Adachi-Pagano, M., Forano, C., & Besse, J. P. (2003). Synthesis of Al-rich hydrotalcite-like compounds by using the urea hydrolysis reaction—control of size and morphology. *Journal of Materials Chemistry, 13*(8), 1988–1993. https://doi.org/10.1039/b302747n

Adam, J., Moreno, J., Bonilla, M., & Pellicer, T. (2016). Classification of damage to the structures of buildings in towns in coastal areas. *Engineering Failure Analysis, 70*, 212–221. https://doi.org/10.1016/j.engfailanal.2016.09.004

Ahmed, I. M., & Gasser, M. S. (2012). Adsorption study of anionic reactive dye from aqueous solution to Mg–Fe–CO3 layered double hydroxide (LDH). *Applied Surface Science, 259*, 650–656. https://doi.org/10.1016/j.apsusc.2012.07.092

Ai, L., Zhang, C., & Meng, L. (2011). Adsorption of Methyl Orange from Aqueous Solution on Hydrothermal Synthesized Mg–Al Layered Double Hydroxide. *Journal of Chemical & Engineering Data, 56*(11), 4217–4225. https://doi.org/10.1021/je200743u

Bakr, A., Mostafa, M., & Sultan, E. (2016). Mn(II) removal from aqueous solutions by Co/Mo layered double hydroxide: Kinetics and thermodynamics. *Egyptian Journal of Petroleum, 25*(2), 171–181. https://doi.org/10.1016/j.ejpe.2015.04.002

Bakr, A., Sayed, N., Salama, T., Ali, I., Gayed, R., & Negm, N. (2018). Potential of Mg–Zn–Al layered double hydroxide (LDH)/montmorillonite nanocomposite in remediation of wastewater containing manganese ions. *Research on Chemical Intermediates, 44*(1), 389–405. https://doi.org/10.1007/s11164-017-3110-5

Cao, Y., Dong, S., Zheng, D., Wang, J., Zhang, X., Du, R., Song, G., & Lin, C. (2017). Multifunctional inhibition based on layered double hydroxides to comprehensively control corrosion of carbon steel in concrete. *Corrosion Science, 126*, 166–179. https://doi.org/10.1016/j.corsci.2017.06.026

Chen, C., Zhou, W., Yang, Q., Zhu, L., & Zhu, L. (2014). Sorption characteristics of nitroso diphenylamine (NDPhA) and diphenylamine (DPhA) onto organo-bentonite from aqueous solution. *Chemical Engineering Journal, 240*, 487–493. https://doi.org/10.1016/j.cej.2013.10.099

Chen, M., Cai, Y., Zhang, M., Yu, L., Wu, F., Jiang, J., Yang, H., Bi, R.& Yu, Y. (2021) Novel Ca-SLS-LDH nanocomposites obtained via lignosulfonate modification for corrosion protection of steel bars in simulated concrete pore solution. *Applied Clay Science*, *211*, 106195. https://doi.org/10.1016/j.clay.2021.106195

Christie, A. B., Lee, J., Sutherland, I., & Walls, J. M. (1983). An XPS study of ion-induced compositional changes with group II and group IV compounds. *Applications of Surface Science, 15*(1), 224–237. https://doi.org/10.1016/0378-5963(83)90018-1

Das, J., Sairam Patra, B., Baliarsingh, N., & Parida, K. M. (2007). Calcined Mg–Fe–CO3 LDH as an adsorbent for the removal of selenite. *Journal of Colloid and Interface Science, 316*(2), 216–223. https://doi.org/10.1016/j.jcis.2007.07.082

Daud, M., Hai, A., Banat, F., Wazir, M. B., Habib, M., Bharath, G.& Al-Harthi, M. A. (2019) A review on the recent advances, challenges and future aspect of layered double hydroxides (LDH) – Containing hybrids as promising adsorbents for dyes removal. *Journal of Molecular Liquids*, *288*, 110989. https://doi.org/10.1016/j.molliq.2019.110989

David, A., & Driessche, P. (2011). Mechanism and equivalent circuits in electrochemical impedance spectroscopy. *Electrochimica Acta, 56*(23), 8005–8013. https://doi.org/10.1016/j.electacta.2011.01.067

Demri, B., & Muster, D. (1995). XPS study of some calcium compounds. *Journal of Materials Processing Technology, 55*(3), 311–314. https://doi.org/10.1016/0924-0136(95)02023-3

Dong, Y., Ma, L., & Zhou, Q. (2013). Effect of the incorporation of montmorillonite-layered double hydroxide nano clays on the corrosion protection of epoxy coatings. *Journal of Coatings Technology and Research, 10*(6), 909–921. https://doi.org/10.1007/s11998-013-9519-x

Frost, R., & Rintoul, L. (1996). Lattice vibrations of montmorillonite: an FT Raman and X-ray diffraction study. *Applied Clay Science, 11*(2–4), 171–183. https://doi.org/10.1016/S0169-1317(96)00017-8

Geoffrey, N., & Nicholas, C. (2008). Archaeology of the continental shelf: Marine resources, submerged landscapes and underwater archaeology. *Quaternary Science Reviews, 27*, 23–24. https://doi.org/10.1016/j.quascirev.2008.08.012

Gomes, C., Mir, Z., Sampaio, R., Bastos, A., Tedim, J., Maia, F., Rocha, C., & Ferreira, M. (2020). Use of ZnAl-Layered Double Hydroxide (LDH) to Extend the Service Life of Reinforced Concrete. *Materials, 13*(7), 1769. https://doi.org/10.3390/ma13071769

Guo, X. D., Zhang, L. J., Chen, Y., & Qian, Y. (2009). Core/shell pH-sensitive micelles self-assembled from cholesterol conjugated oligopeptides for anticancer drug delivery. *AIChE Journal, 56*(7), 1922–1931. https://doi.org/10.1002/aic.12119

Haber, J., Stoch, J., & Ungier, L. (1976). X-ray photoelectron spectra of oxygen in oxides of Co, Ni, Fe and Zn. *Journal of Electron Spectroscopy and Related Phenomena, 9*(5), 459–467. https://doi.org/10.1016/0368-2048(76)80064-3

Javadian, S., Darbasizadeh, B., Yousefi, A., Ektefa, F., Dalir, N., & Kakemam, J. (2017). Dye-surfactant aggregates as corrosion inhibitor for mild steel in NaCl medium: Experimental and theoretical studies. *Journal of the Taiwan Institute of Chemical Engineers, 71*, 344–354. https://doi.org/10.1016/j.jtice.2016.11.014

Javadian, S., Yousefi, A., & Neshati, J. (2013). Synergistic effect of mixed cationic and anionic surfactants on the corrosion inhibitor behavior of mild steel in 3.5% NaCl. *Applied Surface Science, 285*, 674–681. https://doi.org/10.1016/j.apsusc.2013.08.109

Jentzsch, P. V., Kampe, B., Ciobotă, V., Rösch, P., & Popp, J. (2013). Inorganic salts in atmospheric particulate matter: Raman spectroscopy as an analytical tool(J). *Spectrochimica Acta Part A: Molecular and Biomolecular Spectroscopy, 115*, 697–708. https://doi.org/10.3390/cmd2010005

Kanezaki, E. (1998). Thermal behavior of the hydrotalcite-like layered structure of Mg and Al-layered double hydroxides with interlayer carbonate by means of in situ powder HTXRD and DTA/TG. *Solid State Ionics, 106*(3), 279–284. https://doi.org/10.1016/S0167-2738(97)00494-3

Odeku, K. (2021). An Analysis of 'Operation Phakisa' to Unlock the Potential of Ocean Resources in South Africa. *Journal of Asian and African Studies, 56*(2), 382–394. https://doi.org/10.1177/0021909620921885

Lecloux, A., & Pirard, J. P. (1979). The importance of standard isotherms in the analysis of adsorption isotherms for determining the porous texture of solids. *Journal of Colloid and Interface Science, 70*(2), 265–281. https://doi.org/10.1016/0021-9797(79)90031-6

Lv, G., Li, Z., Jiang, W. T., Chang, P. H., & Liao, L. (2015). Interlayer configuration of ionic liquids in a Ca-montmorillonite as evidenced by FTIR, TG-DTG, and XRD analyses. *Materials Chemistry and Physics, 162*, 417–424. https://doi.org/10.1016/j.matchemphys.2015.06.008

Lv, L., He, J., Wei, M., Evans, D. G., & Duan, X. (2006). Uptake of chloride ion from aqueous solution by calcined layered double hydroxides: Equilibrium and kinetic studies. *Water Research, 40*(4), 735–743. https://doi.org/10.1016/j.watres.2005.11.043

Machner, A., Zajac, M., Ben Haha, M., Kjellsen, K. O., Geiker, M. R., & De Weerdt, K. (2018). Chloride-binding capacity of hydrotalcite in cement pastes containing dolomite and metakaolin. *Cement and Concrete Research, 107*, 163–181. https://doi.org/10.1016/j.cemconres.2018.02.002

Mir, Z. M., Gomes, C., Bastos, A. C., Sampaio, R., Maia, F., Rocha, C., Tedim, J., Höche, D., Ferreira, M. G. S., & Zheludkevich, M. L. (2021). The Stability and Chloride Entrapping Capacity of ZnAl-NO_2 LDH in High-Alkaline/Cementitious Environment. *Corrosion and Materials Degradation, 2*(1), 78–99. https://doi.org/10.3390/cmd2010005

Miyata, S. (1983). Anion-Exchange Properties of Hydrotalcite-Like Compounds. *Clays and Clay Minerals, 31*(4), 305–311. https://doi.org/10.3390/ma13061426

Oh, K., Ahn, S., Eom, K., Jung, K., & Kwon, H. (2014). Observation of passive films on Fe-20Cr-xNi(x = 0, 10, 20 wt.%) alloys using TEM and Cs-corrected STEM–EELS. *Corrosion Science, 79*, 34–40. https://doi.org/10.1016/j.corsci.2013.10.023

Qiu, L., Chen, W., & Qu, B. (2006). Morphology and thermal stabilization mechanism of LLDPE/MMt and LLDPE/LDH nanocomposites. *Polymer, 47*(3), 922–930. https://doi.org/10.1016/j.polymer.2005.12.017

Rives, V., & Angeles Ulibarri, M. A. (1999). Layered double hydroxides (LDH) intercalated with metal coordination compounds and oxometallates. *Coordination Chemistry Reviews, 181*(1), 61–120. https://doi.org/10.1016/S0010-8545(98)00216-1

Roobottom, H. K., Jenkins, H. D. B., Passmore, J., & Glasser, L. (1999). Thermochemical Radii of Complex Ions. *Journal of Chemical Education, 76*(11), 1570. https://doi.org/10.1021/ed076p1570

Ryu, H. S., Singh, J. K., Lee, H. S., Ismail, M. A., & Park, W. J. (2017). Effect of $LiNO_2$ inhibitor on corrosion characteristics of steel rebar in saturated $Ca(OH)_2$ solution containing NaCl: An electrochemical study. *Construction and Building Materials, 133*, 387–396. https://doi.org/10.1016/j.conbuildmat.2016.12.086

Sing, K. S. W. (1985). Reporting physisorption data for gas/solid systems with special reference to the determination of surface area and porosity (Recommendations 1984). *Pure and Applied Chemistry, 57*(4), 603–619. https://doi.org/10.1351/pac198557040603

Sing, K. S. W. (1989). The use of gas adsorption for the characterization of porous solids. *Colloids and Surfaces, 38*(1), 113–124. https://doi.org/10.1016/0166-6622(89)80148-9

Kim, T. (2009). Efficient management of marine resources in conflict: An empirical study of marine sand mining. *Korea, Journal of Environmental Management, 91*(1), 78–86. https://doi.org/10.1016/j.jenvman.2009.07.006

Tian, R., Zhong, J., Lu, C., & Duan, X. (2018). Hydroxyl-triggered fluorescence for location of inorganic materials in polymer-matrix composites. *Chemical Science, 9*(1), 218–222. https://doi.org/10.1039/c7sc03897f

Tian, Y., Dong, C., Wang, G., Cheng, X., & Li, X. (2019). Zn–Al–NO2 layered double hydroxide as a controlled-release corrosion inhibitor for steel reinforcements. *Materials Letters, 236*, 517–520. https://doi.org/10.1016/j.matlet.2018.10.177

Tonda, S., Kumar, S., Bhardwaj, M., Yadav, P., & Ogale, S. (2018). g-C3N4/NiAl-LDH 2D/2D Hybrid Heterojunction for High-Performance Photocatalytic Reduction of CO_2 into Renewable Fuels. *ACS Applied Materials and Interfaces, 10*(3), 2667–2678. https://doi.org/10.1021/acsami.7b18835

Vaculíková, L., Plevová, E., & Ritz, M. (2019). Characterization of Montmorillonites by Infrared and Raman Spectroscopy for Preparation of Polymer-Clay Nanocomposites. *Journal of Nanoscience and Nanotechnology, 19*(5), 2775–2781. https://doi.org/10.1166/jnn.2019.15877

Valdez, B., Ramirez, J., Eliezer, A., Schorr, M., Ramos, R., & Salinas, R. (2016). Corrosion assessment of infrastructure assets in coastal seas. *Journal of Marine Engineering & Technology, 19*(4), 240–248. https://doi.org/10.1080/20464177.2016.1247635

Varga, G., Somosi, Z., Kónya, Z., Kukovecz, Á., Pálinkó, I., & Szilagyi, I. (2021). A colloid chemistry route for the preparation of hierarchically ordered mesoporous layered double hydroxides using surfactants as sacrificial templates. *Journal of Colloid and Interface Science, 581*, 928–938. https://doi.org/10.1016/j.jcis.2020.08.118

Wang, D., Xiang, B., Liang, Y., Song, S., & Liu, C. (2014). Corrosion control of copper in 3.5 wt.% NaCl Solution by Domperidone: Experimental and Theoretical Study. *Corrosion Science, 85*, 77–86. https://doi.org/10.1016/j.corsci.2014.04.002

Wang, Q., & O'Hare, D. (2012). Recent advances in the synthesis and application of layered double hydroxide (LDH) nanosheets. *Chemical Reviews, 112*(7), 4124–4155. https://doi.org/10.1021/cr200434v

Wang, X., Xu, J.& Song, Y. (2021) Kinetic, thermodynamic and equilibrium studies on chloride adsorption from simulated concrete pore solution by core@shell zeolite-LTA@Mg-Al layered double hydroxides. *Applied Clay Science*, *209*, 106117. https://doi.org/10.1016/j.clay.2021.106117

Wang, Z., Zhao, X. L., Xian, G., Wu, G., Singh Raman, R. K., Al-Saadi, S., & Haque, A. (2017). Long-term durability of basalt- and glass-fibre reinforced polymer (BFRP/GFRP) bars in seawater and sea sand concrete environment. *Construction and Building Materials, 139*, 467–489. https://doi.org/10.1016/j.conbuildmat.2017.02.038

Wu, B., Zuo, J., Dong, B., Xing, F.& Luo, C. (2019) Study on the affinity sequence between inhibitor ions and chloride ions in Mg Al layer double hydroxides and their effects on corrosion protection for carbon steel. *Applied Clay Science*, *180*, 105181. https://doi.org/10.1016/j.clay.2019. https://doi.org/10.1016/j.clay.2019.105181

Xu, J., Song, Y., Tan, Q., & Jiang, L. (2017). Chloride absorption by nitrate, nitrite and aminobenzoate intercalated layered double hydroxides. *Journal of Materials Science, 52*(10), 5908–5916. https://doi.org/10.1007/s10853-017-0826-y

You, Y., Vance, G. F., & Zhao, H. (2001). Selenium adsorption on Mg–Al and Zn–Al layered double hydroxides. *Applied Clay Science, 20*(1), 13–25. https://doi.org/10.1016/S0169-1317(00)00043-0

Yusuf, S., Moheb, A., & Dinari, M. (2021). Green phenol hydroxylation by ultrasonic-assisted synthesized Mg/Cu/Al-LDH catalyst with different molar ratios of Cu^{2+}/Mg^{2+}. *Research on Chemical Intermediates, 47*(4), 1297–1313. https://doi.org/10.1007/s11164-021-04402-0

Zhang, B., Luan, L., Gao, R., Li, F., Li, Y., & Wu, T. (2017). Rapid and effective removal of Cr(VI) from aqueous solution using exfoliated LDH nanosheets. *Colloids and Surfaces A: Physicochemical and Engineering Aspects, 520*, 399–408. https://doi.org/10.1016/j.colsurfa.2017.01.074

Zou, Y., Zhang, R., Wang, L., Xue, K.& Chen, J. (2020) Strong adsorption of phosphate from aqueous solution by zirconium-loaded Ca-montmorillonite. *Applied Clay Science*, *192*, 105638. https://doi.org/10.1016/j.clay.2020.105638

Zubair, M., Daud, M., McKay, G., Shehzad, F., & Al-Harthi, M. A. (2017). Recent progress in layered double hydroxides (LDH)-containing hybrids as adsorbents for water remediation. *Applied Clay Science, 143*, 279–292. https://doi.org/10.1016/j.clay.2017.04.002

Zuo, J., Wu, B., Luo, C., Dong, B., & Xing, F. (2019). Preparation of MgAl layered double hydroxides intercalated with nitrite ions and corrosion protection of steel bars in simulated carbonated concrete pore solution. *Corrosion Science, 152*, 120–129. https://doi.org/10.1016/j.corsci.2019.03.007

https://doi.org/10.1007/s42860-023-00252-6 Published online by Cambridge University Press